

DIGITAL ACCESS TO SCHOLARSHIP AT HARVARD

X-ray Reflectivity Measurements and Landau Theory of Smectic Wetting in Liquid Crystal–Benzyl Alcohol Mixtures

The Harvard community has made this article openly available. Please share how this access benefits you. Your story matters.

Citation	Kellogg, G. J., Peter S. Pershan, E. H. Kawamoto, W. Foster, Moshe Deutsch, and B. M. Ocko. 1995. X-ray reflectivity measurements and Landau theory of smectic wetting in liquid crystal–benzyl alcohol mixtures. Physical Review E 51(5): 4709–4726.
Published Version	doi:10.1103/PhysRevE.51.4709
Accessed	February 18, 2015 10:03:43 PM EST
Citable Link	http://nrs.harvard.edu/urn-3:HUL.InstRepos:10357484
Terms of Use	This article was downloaded from Harvard University's DASH repository, and is made available under the terms and conditions applicable to Other Posted Material, as set forth at http://nrs.harvard.edu/urn-3:HUL.InstRepos:dash.current.terms-of-use#LAA

(Article begins on next page)

X-ray reflectivity measurements and Landau theory of smectic wetting in liquid crystal–benzyl alcohol mixtures

G.J. Kellogg,* P.S. Pershan, E.H. Kawamoto, and W. F. Foster
Department of Physics and Division of Applied Sciences, Harvard University, Cambridge, Massachusetts 02138

Moshe Deutsch
Physics Department, Bar-Ilan University, Ramat-Gan 52100, Israel

B.M. Ocko
Department of Physics, Brookhaven National Laboratory, Upton, New York 11973
(Received 17 October 1994)

Smectic layering has been observed at the free surface of decylcyanobiphenyl (10CB) and dodecylcyanobiphenyl (12CB) and mixtures of 10CB and 12CB with benzyl alcohol (BA). The effect of BA is to suppress the bulk isotropic-smectic transition temperature T_{IA} and surface layer "transition" temperatures T_j, as well as sharpening these surface transitions by reducing the temperature range ΔT over which layers grow. The observed sharpening appears to saturate for concentrations $x \geq 0.118$. A Landau theory for the growth of a single layer j has been developed, in which the free energy contains a term coupling the concentration x to the local smectic order parameter ψ_j such that $F_j \sim x\psi_j^2$. Applying this theory to pure 12CB and eight mixtures of 12CB-BA, we find that the $j = 1 \rightarrow j = 2$ transition is continuous in pure 12CB, but that the addition of small amounts of impurity drives the transition first order.

PACS number(s): 68.10.−m, 78.70.Ck

I. INTRODUCTION

One of the great successes of x-ray specular reflectivity (XSR) has been the observation of surface smectic layering in liquid crystals [1–8]. In smectic layering, roughly sinusoidal mass and electron-density oscillations develop normal to the interface between the nematic (N) or isotropic (I) liquid crystal and the vapor or a solid substrate. The availability of intense x-ray sources has allowed XSR measurements to be carried out to large momentum transfers q_z, obtaining information on correspondingly small spatial length scales $\Delta z \approx 2\pi/q_z$. Although optical reflectivity techniques, such as ellipsometry and Brewster angle microscopy, are sensitive to surface phases, they cannot directly resolve structure on the molecular length scale. For our purposes, applicability of a kinematic approximation also gives XSR some advantage over other techniques, such as forward-recoil electron spectroscopy and x-ray photoelectron spectroscopy, which in principle have comparable spatial resolution, but which do not directly measure the electron distribution $\rho_e(z)$. Offsetting the sensitivity to the electron density profile $\rho_e(z)$ obtained from XSR is the fact that the measured reflectivity $R(q_z)$ is an intensity, and does not contain phase information; this leads to the well-known problem of nonuniqueness of $\rho_e(z)$ for a given $R(q_z)$ [9]. In many cases, physical intuition or other information about the structure is sufficient to determine the most reasonable profile. We will also argue below that, for the current measurements, the exact details of the profile are not important, and that relative changes in the structure can be believed with a high level of confidence.

A significant reason for interest in smectic layering is that it is an example of *wetting*. In this case, the lower-symmetry smectic-A phase appears at an interface of the higher-symmetry I or N phase with a substrate, or at the free surface, as bulk coexistence between phases is approached. The smectic-A phase is characterized by the smectic order parameter $\psi = |\psi|e^{i\phi}$, which measures the amplitude ($|\psi|$) and phase (ϕ) of electron-density oscillations of period d along the direction z:

$$\rho_e(\mathbf{r}) = \overline{\rho_e} + \mathrm{Re}[\psi e^{i(2\pi/d)z}]. \quad (1)$$

The cyanobiphenyl liquid crystals (nCB) exhibit a variety of bulk liquid crystalline phases. These homologs consist of two phenyl rings with a cyano end group on one end and an alkane tail C_nH_{2n+1} on the other; hence the "n" refers to the tail length. For short tail length ($n \leq 7$), when temperature is lowered at constant pressure, the I phase undergoes a first-order transition to the N phase and, on further cooling, the nematic phase crystallizes; there is no smectic phase. For intermediate chain lengths ($8 \leq n < 9$), an additional N-A transition occurs which is either second order or weakly first order. One recent experiment on the cyanobiphenyls suggests that the N-A transition is always weakly first order [10], even for materials with unmeasurably small latent heats, such as 8CB [11]. (A recent study of cyanobiphenyls sug-

*Present address: Department of Materials Science and Engineering, Massachusetts Institute of Technology, Cambridge, MA 02139.

 ©1995 The American Physical Society

gests that the N-A transition is always weakly first order [10], in contrast to the results of a number of heat capacity and x-ray scattering experiments indicating that the N-A transition is second order sufficiently far from the I-N-A triple point [11–13]). The N-A transition is clearly first-order for $n > 9$, while the N phase disappears entirely in 9CB-10CB mixtures with mole fraction $x \approx 0.3$ 10CB; for $n > 9.3$, there are only first-order I-A and A-crystal transitions [14, 11, 15–18].

The surface smectic layering of the nCB series was previously shown to exhibit an analogous dependence on n as the bulk N-A transition temperature T_{NA} is approached from above [3, 7]. This layering is evident in the behavior of a spatially dependent smectic order parameter $\psi(z)$, where z is measured relative to the interface. For shorter-chain molecules (8CB and 9CB), the modeled $\psi(z)$ grows continuously to saturation as reduced temperature $t = (T - T_{NA})/T_{NA} \to 0$, with an exponential penetration $\psi(z) \sim e^{-z/\xi_{\|}(t)}$, where $\xi_{\|} \sim t^{-\nu_{\|}}$, the bulk correlation length measured along the director, i.e., normal to the layers. The divergence of $\xi_{\|}$ in a continuous manner suggests that smectic wetting for these systems is analogous to critical adsorption [19]. For materials with first-order N-A (mixtures of 9CB and 10CB with mole fraction of 9CB $x \leq 0.3$) or I-A (10CB, 11CB, and 12CB) transitions, the evolution of $\psi(z)$ with t becomes progressively more discontinuous, and it appears that the surface is wetted by a finite number of layers before the bulk transition. However, the distinction between continuous and discrete layering could not be unambiguously made in even the longest-chain nCB: the observed width Δt $[t = (T - T_{IA})/T_{IA}]$ of layering transitions in 12CB was apparently nonzero for all measured transitions.

Though we use the term "transitions" to describe the growth of single smectic layers, it is important to recognize that this growth may not be a true phase transition. For example, the growth of smectic order as temperature is decreased could be dominated by the nonlinear temperature dependence of a layering susceptibility in the presence of either a real or effective surface field. Even if the system had a tendency towards a second-order transition, these fields would quench critical fluctuations and formally suppress any real phase transition. This is similar to the effects of external fields on bulk second-order phase transitions between phases of the same symmetry [20]. We note, however, that the formation of a smectic layer at the surface can occur via a *first-order* transition since the presence of an external field does not suppress discontinuities in the order parameter; however, it can give rise to prominent pre- and post-transitional effects on the order parameter. In any case, the term "transition" will be used here as shorthand for the growth of a single smectic layer.

The initial XSR experiments on liquid crystal surfaces that were cited above stimulated the development of a number of approaches to understanding smectic wetting in the mean field approximation. While bulk second-order transitions between the N and A phases are dominated by fluctuations, making mean field theory inapplicable, it should be useful in gaining a qualitative understanding of smectic wetting. For long-chain materials ($n \geq 9$), the bulk N-A or I-A transitions are first order, so that the universal behavior associated with critical phenomena is absent and analytic theories (such as the renormalization group) are inapplicable. Although fluctuation effects may still be important, and although it may be necessary to include them in numerical calculations for either, or both, bulk and surface transitions, the presence of a free surface characterized by surface tension γ does reduce the magnitude of fluctuations at the surface [21].

The first attempt to understand smectic layering consisted of a lattice model using Ising spins to represent smectic and nematic order. The calculation predicted the continuous growth of up to two surface smectic layers at the free interface of the I phase [22]. A density-functional theory [21], using an anisotropic potential similar to that of the original McMillan theory for bulk transitions to the A phase [23], predicted two discontinuous layering transitions for the I phase. A similar density-functional calculation, with additional translational-rotational terms added to the single-particle potential, indicated the continuous growth of 3–4 smectic layers [24]. Recently, the same interparticle interactions were used to study layering in an isotropic fluid at an interface characterized by a long-range potential ($\sim 1/z^3$, $z \equiv$ distance from the interface) [25]. While this calculation is more appropriate for the problem of layering at a solid substrate, an interesting prediction is made in regard to the surface phase diagram. For a particular choice of relative values of surface and bulk interaction parameters, a region of incomplete wetting is found, with a finite number (in this case, 2) of first-order layering transitions terminated by critical points. For other choices of interaction parameters, this incomplete wetting goes over to complete wetting, as expressed by an infinite number of layering transitions. This model does not treat layering of the N phase. None of the approaches discussed here has produced layering in the N phase which is continuous for short chains evolving to first-order transitions in the smectic-A phase, as was inferred from the experimental results, although the recent calculations do suggest that the progression from short to long chains can induce a progression from continuous to first-order layering [25].

In an effort to determine whether layers grow continuously or with a discrete jump in the local smectic order parameter of layer j, ψ_j, XSR data for the temperature region surrounding the growth of a single layer, $j = 2$, have been modeled by electron-density profiles whose parameters are a measure of the amplitude of the electron-density oscillation of the surface smectic layers. Two materials were studied with direct I-A transitions, 10CB and 12CB, as well as mixtures of these liquid crystals with benzyl alcohol, C_7H_8O (BA). It is well known that, although the presence of small amounts of impurity does not change the topology of a thermal equilibrium phase diagram, it can both shift the phase boundaries and change the order of transitions [20, 26]. By comparing the systematic behavior of mixtures as a function of solute concentration it is possible to gain greater insight into the behavior of the pure materials. By way of illustration, it has been shown that small amounts of im-

purity can dramatically alter the wetting properties of binary liquids [27, 28]. The measurements we report below are a demonstration of the qualitative and quantitative significance of impurities in the smectic wetting of liquid crystals, and in particular suggest that the $j = 1 \rightarrow j = 2$ transition in pure 12CB is continuous, but is driven first order by small concentrations of BA.

II. REFLECTIVITY THEORY AND ELECTRON-DENSITY MODEL

The principles of x-ray specular reflectivity have been described in a number of publications [29, 1, 7], and we present here the important relationships without development. The primary results of interest are the Born approximation expression for the reflectivity due to structure normal to the interface and the effects of surface roughness, here due to thermally excited capillary waves.

For an infinitely sharp interface between vacuum or air and homogeneous matter, unpolarized x rays are specularly reflected with an intensity described by the usual Fresnel form familiar from classical electromagnetic wave theory [29, 7],

$$R_F(q_z) \approx \left| \frac{q_z - (q_z^2 - q_c^2)^{\frac{1}{2}}}{q_z + (q_z^2 - q_c^2)^{\frac{1}{2}}} \right|^2, \quad q_z > q_c. \tag{2}$$

Here, q_z is the momentum transfer normal to the interface and $q_c \approx 4\sqrt{\overline{\rho_e} r_0 \pi}$ is the critical wave vector, such that $R_F(q_z \leq q_c) = 1$. With an average bulk electron density of $\overline{\rho_e} = 3.2 \times 10^{23}$ cm^{-3} (typical of hydrocarbons) and $r_0 = 2.818 \times 10^{-13}$ cm, $q_c = 0.021$ Å^{-1}.

Real surfaces have structure, both normal to and within the plane defining them. Both cases can be treated within the Born approximation if the angle of incidence is large compared to the critical angle so that refraction effects can be neglected and the scattering is weak. If one expresses the structure in the z direction averaged over the coherence length of the x rays within the plane as $\rho_e(z)$, the reflectivity is given by

$$R(q_z) = |\Phi(q_z)|^2 R_F(q_z), \tag{3}$$

with

$$\Phi(q_z) = \frac{1}{\overline{\rho_e}} \int_{-\infty}^{\infty} dz e^{-iq_z z} \frac{\partial \rho_e(z)}{\partial z}. \tag{4}$$

For the case of a fluctuating or rough interface, additional scattering arises at $q_z, \mathbf{q}_\perp \neq \mathbf{0}$, where $\mathbf{q}_\perp$ lies *within* the plane of the surface. This *diffuse scattering* will not be discussed in detail here. It is clear, however, that diffuse scattering will be accompanied by decrease in the magnitude of the specularly reflected radiation relative to that from a sharp interface. It can be shown that the effect of diffuse scattering by thermal capillary waves, which are present at all liquid-vapor interfaces, decreases the specular signal in a manner reminiscent of the Debye-Waller factor in bulk diffraction which arises from thermal fluctuations [30, 31]:

$$\frac{R}{R_F} = |\Phi(q_z)|^2 e^{-q_z^2 \sigma_C^2}, \tag{5}$$

where σ_C is the root-mean-square roughness due to capillary waves. The value of σ_C is determined by the temperature, surface tension, and the long-wavelength $q_{\min}$ and short-wavelength $q_{\max}$ cutoffs in the capillary wave spectrum [32, 33]. It has been observed that although $q_{\min}$ is determined by the projection of the reflectometer resolution on the plane of the surface, in all practical experiments the reflectivity can be modeled by implicitly treating the interfacial widths of the model as a combination of the intrinsics widths (e.g., the inherent width σ_0 of the liquid-vapor interface) and the capillary wave roughness [34]. By modeling reflectivities from liquid surfaces in this way, it has been found that a consistent and physically meaningful choice for the short-wavelength capillary wave cutoff is $q_{\max} \approx \pi/a$, where a is the molecular diameter.

To represent smectic layers at the surface of an isotropic liquid crystal, a model electron-density profile is needed that can capture the nearly sinusoidal oscillations of bulk smectic-A liquid crystals while at the same time allowing the smectic order parameter ψ_j of the jth layer to vary as a function of temperature. This is a generalization of the sinusoidal model previously employed, which consisted of a sine-wave oscillation about the bulk electron density $\overline{\rho_e}$ penetrating a fixed distance into the bulk [3]. This ability to model varying amplitudes is especially important in regions where the transition $j \rightarrow j + 1$ layers occurs: if these transitions are continuous, one must be able to model smectic order for the $j + 1$ layer that is intermediate between the I phase ($\psi_{j+1} = 0$) and a saturation level.

The model consists of an error-function interface, with electron density rising from zero to $\overline{\rho_e}$, representing the transition from the vapor to the liquid. To this are added oscillatory layers with zero net integrated electron density. Each layer j consists of a central, positive Gaussian of amplitude $\overline{\rho_e} A_j$ at position $z_j = z_0 + (j - 1)d$, with two negative Gaussians of amplitude $-\frac{1}{2}\overline{\rho_e} A_j$ at positions $z_j \pm d/2$; here, z_0 is an offset from the surface defined by the error function and d is the smectic layer spacing. Bulk diffraction studies on nCB's are consistent with a smectic-A structure where the molecules pair head to head to form a bilayer which is the repeat unit of the one-dimensional density oscillation [35]. The positive Gaussian in the model can be thought of as representing the overlapping molecular cores of the bilayer and the negative Gaussians the lower density tails. Explicitly,

$$\begin{aligned} \rho_e(z) = {} & \tfrac{1}{2}\overline{\rho_e}[\mathrm{erf}(z/\sqrt{2}\sigma_s) + 1] \\ & + \overline{\rho_e} \sum_{j=1}^{j=n} A_j [-\tfrac{1}{2} e^{-\frac{1}{2}(z_j + \frac{1}{2}d)^2/\sigma_l^2} + e^{-\frac{1}{2}z_j^2/\sigma_l^2} \\ & - \tfrac{1}{2} e^{-\frac{1}{2}(z_j - \frac{1}{2}d)^2/\sigma_l^2}], \end{aligned} \tag{6}$$

where σ_s is the *Gaussian width* of the surface profile, made up of both surface roughness and intrinsic width, and σ_l represents a similar quantity for the individual layers.

It is important to realize that the exact nature of the model is not of great significance in the current study. The primary requirement is the ability to describe a single layer's change in smectic amplitude as a function of temperature; even if the independent-layer model does not represent the exact *quantitative* features of the structure, the *relative* changes in smectic order are well represented. This can be seen in that good fits can be made using the model where the only parameters with significant temperature dependence are the A_j. For this reason we use the A_j to represent the layer smectic order parameter ψ_j.

III. EXPERIMENTAL DETAILS

A. Sample cells and sample preparation

To minimize temperature gradients across the samples which could smear transitions, the aluminum cells shown in Fig. 1 were built. These cells were made with the smallest x-ray windows which could safely accommodate the specular beam at all angles, measuring 9.5 mm × 10 mm; the windows themselves were made of 0.25 mm thick beryllium foil (to increase thermal conductivity), sealed to the body of the cell with zero-volume indium O rings. The cells were also designed to have a very small free volume, with a space of approximately 6 mm above the surface of the liquid. The liquid crystals themselves form a large puddle 0.1–0.3 mm thick on top of a 7.6 cm diam × 3.2 mm thick polished silicon wafer. Silicon was used rather than glass because its thermal conductivity ($K_T \approx 1.7$ W cm^{-1} K^{-1}) is more than two orders of magnitude greater than that of glass ($K_T \approx 9 \times 10^{-3}$ W cm^{-1} K^{-1}).

These cells formed the inner stage of a two-stage temperature-controlled oven. The outer can consisted of a brass cylinder with 3.2 mm walls and a brass lid. Small kapton windows insured a dead space between the outer can and the inner cell. Temperature control was maintained to ±0.5 mK at the sample, with a YSI Model 72 temperature controller on the outer can and a custom-built temperature controller for the inner cell; YSI 44011 thermistors were used for both control and temperature

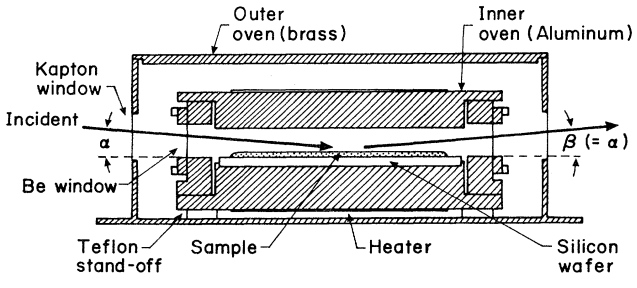

FIG. 1. Sample cell used for 12CB and 12CB-BA experiments; details of the construction are described in the text. Also shown is the path of the x-ray beam specularly reflected and grazing angles of incidence α and reflection β.

measurement. The temperature gradient was found to be $|\Delta T| \leq 5$ mK between the edge of the sample wafer and the center of the cell.

In all cases, the silicon substrate was precleaned in a H_2SO_4-H_2O_2 bath and rinsed with deionized, purified water. After blowing the disk dry with dry nitrogen, it was placed in the inner cell. For the experiments using pure liquid crystals, they were added directly from the bottle without further purification.

Baker Analyzed benzyl alcohol (C_7H_8O) (BA) was used in the mixture experiments. In these experiments, BA was added to a known weight of liquid crystal using a microliter syringe; the sealed mixing bottle was heated to melt the sample, which was then placed in an ultrasonic water bath for 5 min. The mixtures were then added to the hot silicon wafer in the liquid state; if any evidence of phase separation was observed, the sample was removed. We found through the course of these experiments that phase-separated samples could not be restored to a homogeneous state, even with heating as high as 80 °C. This is not surprising, considering the small diffusion constants of solutes in liquid crystals [36] and the thinness of the puddles.

Finally, it should be noted that the thinness of the liquid puddles acts to cutoff low-frequency, long-wavelength gravity waves caused by room vibrations. The macroscopic flatness (or low figure error) of these samples is demonstrated by the ability to measure a specular signal to very high angles.

B. X-ray measurements

Extensive use of both the Harvard rotating anode x-ray source and beamline X22B at the National Synchrotron Light Source (NSLS) was made in acquiring the data. Both are equipped with special spectrometers built to allow scattering measurements from horizontal liquid surfaces and have been described in detail elsewhere [37, 7]. In terms of the kinematics of reflectivity, the spectrometers are identical. As the incident grazing angle α is increased by tilting down the x-ray beam reflected from a monochromator, the sample is lowered by an elevator; the specular beam is reflected at angle $\beta = \alpha$. Associated with α is a divergence $\Delta\alpha$ due to x-ray slit sizes (and, at the synchrotron, the inherent divergence of the source). The size of the detector slit determines the detector resolution $\Delta\beta$. The outgoing slits were set to allow all of the specularly reflected x-ray radiation to enter the detector; as explained elsewhere [5], this implies that for a flat surface the resolution Δq_z is dominated by the incident resolution $\Delta\alpha$. For the Harvard and NSLS spectrometers these resolutions were $\Delta q_z \approx 4\pi\Delta\alpha/\lambda \leq 2.6 \times 10^{-4}$ Å^{-1}.

All data on mixtures of 12CB with BA were taken at Harvard, with $\lambda = 1.5405$ Å. The pure 12CB data were taken at NSLS with a wavelength of $\lambda = 1.5567$ Å. Data on pure 10CB and 10CB-BA mixtures were taken at NSLS with $\lambda = 1.5295$ Å and $\lambda = 1.5374$ Å.

A common background-subtraction procedure was used for all measurements. Because the intensity measured at the specular condition consists of the specular signal, stray background, and surface and bulk diffuse

scattering which fall within the detector resolution, it is desirable to remove as much of the nonspecular scattering as possible. If the momentum transfer is defined as $\mathbf{q} = (q_x, q_y, q_z)$, with q_x the momentum transfer within both the plane of the surface and the reflection plane and q_y orthogonal to q_x and q_z, then background subtraction should be performed at the smallest values of $q_\perp = \sqrt{q_x^2 + q_y^2}$ which are practical. Unfortunately, for practical values of the reflectometer resolution, the fraction of the total diffuse scattering due to thermal capillary waves which lies under the specular peak is quite large. This is because capillary wave diffuse scattering is proportional to $1/q_\perp^2$ so long as $q_\perp \lambda_{surf} \gg 1$, where $\lambda_{surf} \approx 2$ cm is the capillary wavelength. Because significant amounts of diffuse scattering cannot be subtracted away from the specular signal, the background was taken as the average intensity of two points $\mathbf{q} = (q_x = \pm q_z/300, q_y = 0, q_z)$ well away from the specular peak, to avoid inadvertently subtracting any of the reflectivity signal. While this widely used procedure does not fully separate the diffuse scattering from the specular signal, in almost all cases it yields a reflectivity curve for which the effects of roughness can be well described by a Debye-Waller-like factor with an effective, q_z-independent value of σ_C.

IV. RESULTS

Reflectivity measurements as a function of q_z and T, $R(q_z, T)$, were performed on samples of pure 12CB, pure 10CB, and mixtures of both materials with BA. As will be shown below, layer transitions as a function of temperature can be characterized by a combination of these measurements and a restricted set of temperature measurements, $R(q_z^*, T)$, at a fixed wave vector $q_z^* \approx 0.925 q_0$ ($q_0 = 2\pi/d$); in terms of reduced temperature $t = (T - T_{IA})/T_{IA}$, the latter measurements are denoted $R(q_z^*, t)$. The measurements $R(q_z^*, T)$ were used in two ways. First, constant rate transition temperature drifts of a few mK/h are ubiquitous in liquid crystals; this drift was apparent in a shift ΔT in the temperature dependence of features in $R(q_z^*, T)$. The shift ΔT of a curve with respect to one measured at an earlier time was used to generate a corrected bulk transition temperature, $T_{IA} \rightarrow T_{IA} + \Delta T$. This in turn provides a corrected reduced temperature. When adjusted in this way, two curves with a temperature shift collapse almost identically onto one another. This gives us confidence temperature dependence of the surface structure remained consistent over the course of the measurement. By repeatedly measuring $R(q_z^*, T)$ we have corrected the reduced temperatures of full reflectivity measurements taken over the course of several hours to several days on a single sample. The second use of $R(q_z^*, T)$ was to generate A_2 values in the model of Eq. (6) at temperatures between those of full reflectivity measurements $R(q_z, T)$ through an interpolation process which will be described below.

The procedure followed for each sample was to measure $R(q_z^*, T)$ several times at the beginning of the experiment. When a constant drift had been achieved, specular reflectivities $R(q_z, T)$ were measured in the region of $j = 1 \rightarrow j = 2$. A measurement of $R(q_z^*, T)$ was performed before and after each full reflectivity. For all materials, $R(q_z^*, T)$ was measured by changing the temperature and allowing the reflected intensity to stabilize, assuring that at each temperature the surface structure had equilibrated. Both descending and ascending data were measured. No sample showed hysteresis, to within the ± 5 mK afforded by the measurement.

In order to determine the reduced temperature t, the bulk transition temperature T_{IA} was measured for each sample after all reflectivity measurements were performed. In each case, T_{IA} was determined by translating the sample through the beam with fixed angles $\alpha \neq \beta$ such that $\mathbf{q} = (q_0/300, 0, q_0)$ while lowering the temperature in 5 mK increments near the transition. This allowed for discrimination against the specular signal, both from the surface and from bulk domains oriented with layers parallel to the surface. With each change in temperature, at least 10 min were allowed for equilibration; constant intensity was also used as an indicator of equilibrium. A sudden increase in intensity (of more than two orders of magnitude) as well as the development of a non-resolution-limited peak (signaling smectic domains with a spread of layer normals) were taken as indicators of the transition to the bulk A phase.

A. 12CB and 12CB-BA mixtures

For the pure 12CB sample, the bulk transition temperature was measured to be $T_{IA} = 58.086 \pm 0.005\,^\circ$C (331.236 K). This is the value for a particular sample after a period of drift, and does not represent the value extrapolated back to the time of the introduction of the sample to the scattering cell.

Full specular reflectivities were measured at twelve reduced temperatures in the $j = 1 \rightarrow j = 2$ region. Figure 2 shows two normalized reflectivities R/R_F and model fits, for temperatures just below and just above the feature in $R(q_z^* = 0.15\ \text{Å}^{-1}, t)$ associated with the growth of the second layer. The increase in intensity at $q_z^* = 0.15\ \text{Å}^{-1}$ in R/R_F can be seen in the inset of Fig. 2, where $R(0.15\ \text{Å}^{-1}, t)$ is displayed. The "steps" signal the localized addition of layers.

For these measurements, we have found that good fits to the data can be made using an electron density as expressed by Eq. (6). The behavior of the parameters is as follows

First, all 12CB, 12CB-BA, 10CB, and 10CB-BA reflectivities were fitted with the layer roughness fixed at $\sigma_l = 5.0$ Å. We found that we could vary this parameter from $\sigma_l \approx 0.5$ Å to $\sigma_l \approx 8.0$ Å without noticeable changes in the quality of the fits. We attribute this to the fact that the limited range in q_z measured in these experiments was not sufficient to determine short-length-scale variations in $\rho_e(z)$.

For pure 12CB, all parameters other than the layer amplitudes A_j show very little temperature dependence, with the exception of the layer spacing d. An abrupt

change from $d = 36.74 \pm 0.14$ Å to $d = 38.28 \pm 0.09$ Å occurs upon second layer formation. The reflectivity modeled by Eq. (6) is quite sensitive to d; the combination of thickness and offset z_0 determines the position of the interference minimum. The possibility that this change in apparent layer thickness was due to *different* thicknesses for the first and second layers was explored by allowing the two length scales to independently vary; the uncertainties associated with these fits were so large as to make the two lengths indistinguishable. Fixing the thickness at the average value of $\overline{d} = 37.51$ Å resulted in poorer fits, with the goodness-of-fit parameter χ^2 increasing by approximately a factor of 2 for data well above and well below the transition. We note that all fitted values are smaller than the bulk value of $d = 39.15$ Å.

The position of the center of the first bilayer, z_0, was found to be nearly constant, $\overline{z_0} = 19.70 \pm 0.04$ Å. Fits with constant z_0 yielded identical results to within the quoted errors as the fits allowing z_0 to float. This value is almost exactly $d/2$ for the bulk, but is somewhat larger than $d/2$ for the surface layers ($\overline{z_0} = 0.515\overline{d}$ for $j = 2$, $\overline{z_0} = 0.525\overline{d}$ for $j = 1$).

The surface roughness σ_s shows some systematic variation with t, from a high value of 5.05 ± 0.05 Å at low temperatures to a low value of 4.89 ± 0.04 Å at high temperatures. Fixing the roughness at the average value resulted in an increase in χ^2 of 10–20 % for low temperature and high temperature fits. Apparently, the growth of a second smectic layer does not significantly alter the microscopic roughness or intrinsic width of the interface.

Figure 3 shows the fitted layer amplitudes A_1, A_2, and A_3 as a function of reduced temperature for pure 12CB. (Also shown is $x_0 = 0.263$ BA in 12CB, to be discussed below.) As expected, the second-layer amplitude A_2 undergoes the largest change with temperature, from $A_2 \approx 0.022$ at the highest temperature to $A_2 \approx 0.09$ at the lowest temperature. Amplitude A_1 is nearly constant, with average value $\overline{A_1} = 0.127$. We attribute the scatter in A_1 to systematic errors and/or correlations between the fitting parameters. Fixing A_1 at the average value increases χ^2 by $\leq 30\%$. Finally, A_3 is nearly zero. Fixing $A_3 = 0$ results in an increase in χ^2 of $\approx 50\%$ for the low temperature data.

In addition to pure 12CB, samples containing BA at eight different concentrations were measured. The concentrations (weight percentages) studied were x_0= 0.031(1%), x_0=0.076(2.5%), x_0=0.090(3%), x_0= 0.118(4%), x_0=0.145(5%), x_0=0.170(6%), x_0= 0.207(7.5%), and x_0=0.263(10%). Samples with larger concentrations of BA were not measured in detail be-

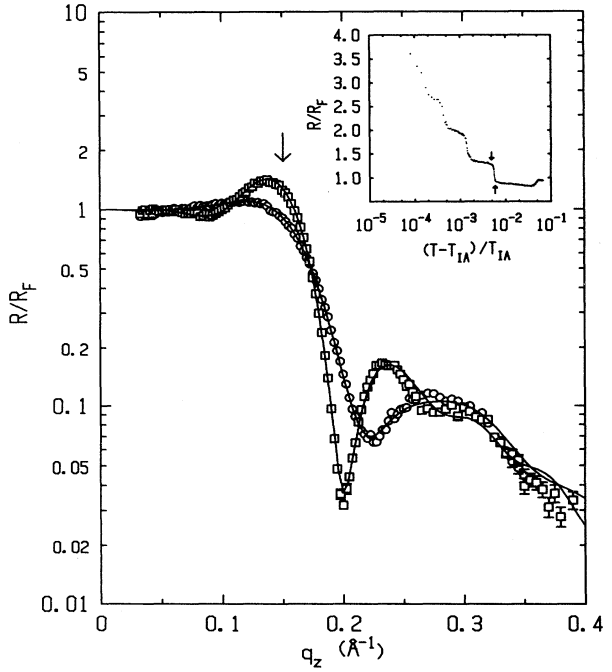

FIG. 2. X-ray specular reflectivity of pure 12CB at a reduced temperatures $t = 5.98 \times 10^{-3}$ (○) and $t = 4.96 \times 10^{-3}$ (□). The solid lines are fits to the independent-layer model discussed in the text. The inset shows $R(0.15\ \text{Å}^{-1}, t)$, taken at $q_z = 0.15\ \text{Å}^{-1}$ marked by the arrows on the reflectivity plot. The temperatures of the reflectivities are shown as well in the inset, illustrating the "step" which corresponds to $j = 1 \rightarrow j = 2$.

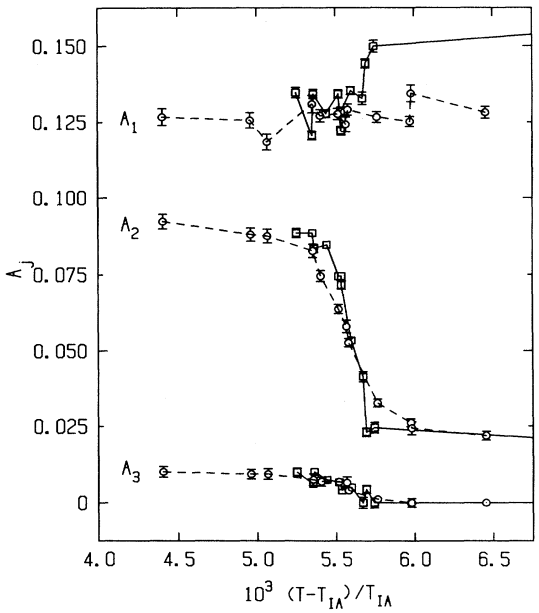

FIG. 3. Layer amplitudes for A_j pure 12CB (○) and $x_0 = 0.263$ BA (□) in 12CB as obtained from fits to the independent-layer model discussed in the text. The reduced transition temperatures $t_2 \equiv (T_2 - T_{IA})/T_{IA}$ are not equal for pure 12CB and the mixture and the 12CB-BA curve has been offset by $\Delta t = 7 \times 10^{-4}$ to increase the clarity of the comparison. The "sharpening" of $j = 1 \rightarrow j = 2$ is clearly evident. The fact that amplitudes A_1 and A_3 show very little change in the temperature region of $n = 2$ formation suggests that a Landau theory ignoring explicit coupling of A_2 to these parameters may be applicable. The lines are guides to the eye.

cause neither $R(0.15\ \text{Å}^{-1}, T)$ nor T_{IA} stabilized over the course of several days.

For the mixtures listed, the curves $R(0.15\ \text{Å}^{-1}, T)$ were measured and bulk transition temperatures were measured. Also measured were a number of specular reflectivities, one at a temperature below T_2 and one above T_2 for most samples; for the $x_0 = 0.145$ sample, reflectivities were measured at 12 temperatures in the vicinity of $j = 1 \rightarrow j = 2$. The reflectivities could be fitted with curves generated by the electron-density model Eq. (6) with parameters that did not significantly differ from those used for pure 12CB; these reflectivities will be discussed in Sec. V. Two significant effects are apparent from the $R(0.15\ \text{Å}^{-1}, T)$ data alone. First, there is a dramatic suppression of the bulk (T_{IA}) and surface (T_j) transition temperatures; this is shown for T_{IA} and T_2 in Fig. 4. Second, there is an apparent "sharpening" of the transitions $j \rightarrow j + 1$. This is quite dramatic for the larger concentrations, as can be seen in Fig. 5, where $R(0.15\ \text{Å}^{-1}, t)$ is plotted for pure 12CB and $x_0 = 0.263$ BA in 12CB. This sharpening increases as concentration is increased to $x_0 = 0.145$; for higher concentrations, the shape of $R(0.15\ \text{Å}^{-1}, T)$ remains virtually unchanged and could be described as a step function with some temperature smearing, as well as small pre- and post-transitional tails.

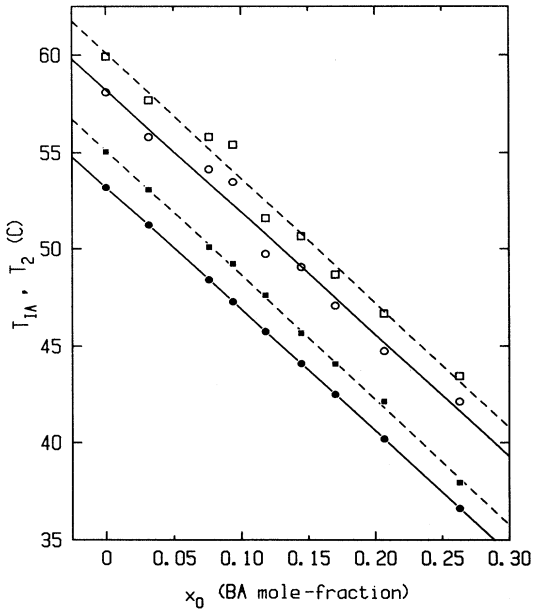

FIG. 4. Bulk I-A transition temperatures T_{IA} (○) and second-layer transition temperature T_2 (□) for nine concentrations of BA in 12CB, shown with linear fits in the upper part of the figure. The fits have a slope of $dT_{IA}/dx = -64 \pm 3.0$ K/mole fraction. The scatter in the points is presumably due to systematic errors in determining the concentrations, since solid squares indicate where the T_2 would appear if the concentrations were adjusted to such that data for T_{IA} fall on the solid line. (Both T_{IA} and T_2 for this adjustment have been shifted for clarity.) The difference $T_2 - T_{IA}$ is nearly constant, $T_2 - T_{IA} \approx 1.77$ K.

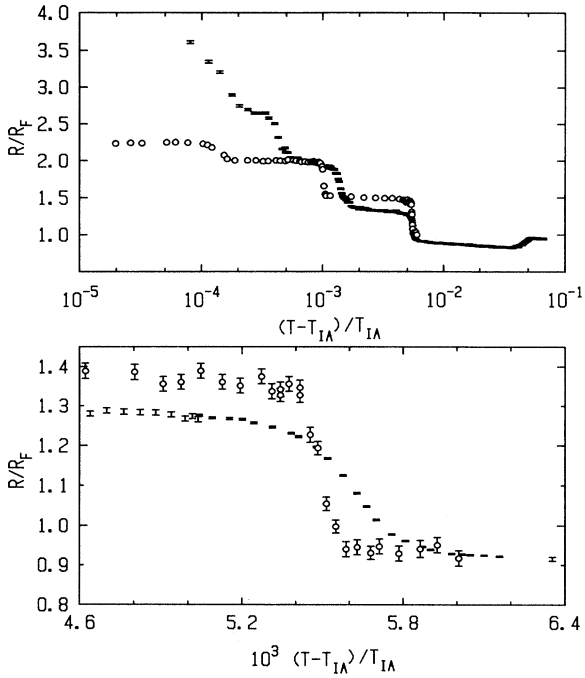

FIG. 5. Reflectivity $R(0.15\ \text{Å}^{-1}, t)$ at fixed $q_z = 0.15\ \text{Å}^{-1}$ for pure 12CB (·) and $x_0 = 0.263$ BA in 12CB (○).

The surface transition temperatures T_j were determined by fitting $R(0.15\ \text{Å}^{-1}, T)$ in the region of the transition to a form consisting of an error function centered at T_j, with additional constant and linear background terms. Though we do not expect this specific form to have any physical significance, the fitted values of T_j should be relatively accurate.

Table I lists T_{IA} and T_j as a function of x_0. The T_{IA} results were reproduced by observing the onset of birefringence for samples in sealed glass capillaries submerged in a water bath with ±0.1 °C temperature control. The transition temperatures measured in this way were found to be stable to within ±0.1 °C after an short initial period of drift, and no evidence of demixing was observed for periods of up to two weeks.

While there is some scatter in the data of Fig. 4, the suppression of both T_{IA} and T_2 is primarily linear in x_0. A linear fit for T_{IA} gives $dT_{IA}/dx_0 = -63.9 \pm 2.7$ K/mole fraction, and for T_2 $dT_2/dx_0 = -64.3 \pm 2.8$. The residuals for T_{IA}, $\Delta T = T_{fit} - T_{IA}$, are large for $x_0 = 0.076$ ($\Delta T = 0.74$ K), $x_0 = 0.09$ ($\Delta T = 1.20$ K), and $x_0 = 0.118$ ($\Delta T = -1.00$ K), but $|\Delta T| \leq 0.55$ K for the remainder. We attribute the scatter primarily to uncertainties in the initial concentration x_0, but also to temperature drifts. As $R(0.15\ \text{Å}^{-1}, T)$ was measured repeatedly for a sample, T_2 was observed to drift; after an initial drift of $d(T_2)/dt \sim -10$ to -20 mK/h, a steady-state drift of $|d(T_2)/dt| \leq 2$ mK/h would obtain after 6–12 h. Because the drift was usually positive, we attribute this to loss

of BA, possibly through transport through the vapor to the inner surfaces of the cell, loss of vapor through poor O-ring seals, or slow phase separation in which a BA-poor region developed at the surface. In any case, the measurements for T_2 quoted are those corresponding to a measurement of T_{IA} which immediately followed, to minimize the intervening drift. The bulk transition temperature was usually measured only once, at the end of the reflectivity measurements, because it became clear that the appearance of a significant amount of bulk smectic led to phase separation, as evidenced by a large positive shift in T_2 and T_{IA} upon reheating.

While the effects of drifts or uncertainty in x_0 introduce significant error in the values of T_{IA} and T_2, their relative values appear to have much less sample-to-sample variation, as we would expect. The difference $T_2 - T_{IA}$ is nearly constant, with an average value $T_2 - T_{IA} = 1.77$ K. Though the scatter in $T_2 - T_{IA}$ is smaller than that in linear fits to either of these temperatures as a function of x_0, it is still large, with a standard deviation of $\sigma_T \approx 0.13$ K. This is significantly larger than what one would expect from the uncertainties in the measurements of T_{IA} and T_2, the combined errors from which, even in the presence of (corrected) drifts, should be $\Delta T \leq 0.02$ K. The origin of this scatter is uncertain, but one possibility is a difference between the local concentrations in the surface region, where T_2 was measured, and the bulk, where T_{IA} is determined. This difference may vary randomly from sample to sample. Because of the large fluctuations in $T_2 - T_{IA}$, any small trends would be difficult to determine.

TABLE I. 12CB-BA bulk transition and layer transition temperatures. The bulk transition temperatures T_{IA} for concentrations x_0 of BA in 12CB are listed with the layering temperatures T_i and reduced temperatures of layering t_i for layers 1–5 (where measured). The true reduced temperatures are $10^{-3}\times$ the values shown, e.g., $4.7 \rightarrow 4.7 \times 10^{-3}$. The uncertainty in the values shown is $\Delta T \approx \pm 0.005\,^{\circ}$C; in reduced temperature, $\Delta t \approx \pm 10^{-4}$.

x_0	T_{IA}	T_1/t_1	T_2/t_2	T_3/t_3	T_4/t_4	T_5/t_5
0	58.086	73.7	59.930	58.533	58.266	58.122
		47	5.57	1.35	0.42	0.011
0.031	55.815		57.672	56.258	55.926	55.857
			5.64	1.36	0.33	0.013
0.076	54.146		55.810			
			5.08			
0.090	53.490		55.418	53.930	53.594	53.5
			5.90	1.35	0.32	0.003
0.118	49.735		51.579			
			5.71			
0.145	49.057		50.637			
			4.90			
0.170	47.086		48.672	47.419	47.166	
			4.95	1.04	0.25	
0.207	44.747		46.676	45.153	44.833	
			6.07	1.28	0.43	
0.263	41.710		43.439	42.028	41.761	
			5.49	1.01	0.16	

The linear dependence shows that 12CB and BA follow Raoult's law for ideal solutions [38]. This is also in accordance with the Landau theory coupling ψ and x_0 which we present below.

All samples with concentrations up to $x_0 = 0.145$ were found to have a homogeneous surface phase at temperatures in the vicinity of the $j = 1 \rightarrow j = 2$ transition. This was determined by translating the sample through the beam at $q_z = 0.15$ Å^{-1} with narrow vertical incident slits, so that a small x-ray footprint traversed the sample. These scans yielded flat intensities over the sample, even at temperatures in the center of the transition; we conclude from this that all parts of the sample surface possessed the same structure at a given temperature. Scans of the detector vertically through the reflected beam were also performed with a small x-ray footprint located at five positions along the length of the sample. These scans showed no broadening relative to scans taken at high temperatures or in the plateau regions where there was very little dependence of reflectivity on temperature; the reflected beam was also observed to be centered at the correct position for reflection from a horizontal surface. The combination of sample and detector scans shows that the surface was macroscopically flat over almost 70 mm for most samples.

Sample scans for $x_0 \geq 0.170$ were flat in the plateau regions, but showed characteristic shapes in the vicinity of the layering transitions. Figure 6 shows six scans for $x_0 = 0.263(10\%)$ in the vicinity of the the $j = 1 \rightarrow j = 2$ transition with an x-ray footprint of 2.7 mm along the beam direction and 5 mm in the transverse direction. These and other scans at interleaving temperatures show a smooth evolution from flat scans to nonuniform scans in the region of the transition, and finally flat scans at the other side of the transition. As with the lower concentrations, detector height scans taken with the x-ray spot on different parts of the sample in the center of the transition showed no broadening relative to scans in the plateaus, and the reflected beam was in the correct position for specular reflection from a flat surface. This indicates that the observed intensity variation is not the effect of macroscopic distortions of the surface (figure error). From quantitative analysis of the data represented in the figure it is clear that, over the most of the sample, the reflected intensity could be described as $R(0.15\ \text{Å}^{-1}, T)_X = R(0.15\ \text{Å}^{-1}, T - T_{eff}(X))$, where X is the longitudinal position of the x-ray spot and $T - T_{eff}(X)$ appears to vary by a few tenths of a degree across the sample. It is also clear that $dT_{eff}(X)/dX$ is approximately linear across most of the sample. From the slope of the linear region in the $T = 43.182\,^{\circ}$C curve of Fig. 6, this can be estimated as $|dT_{eff}(X)/dX| \approx 1.4$ mK/mm.

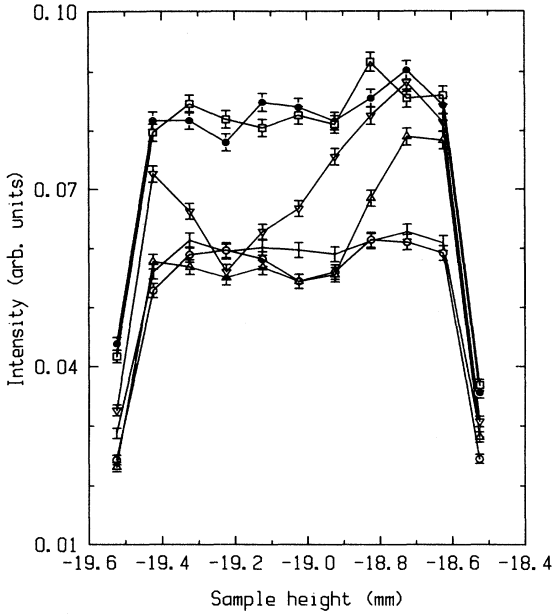

FIG. 6. Intensity reflected from the surface of a 12CB sample, with $x_0 = 0.263$ BA, as the sample is translated through the incident beam. Shown are reflectivities at eight temperatures in the vicinity of $j = 1 \rightarrow j = 2$: $T = 43.42\,^{\circ}$C (·), 43.352 °C (○), 43.246 °C (△), 43.182 °C (▽), 43.112 °C (•), 43.078 °C (□). The shape of the scans in the center of the transition shows that the local layering transition temperature varies across the surface of the sample.

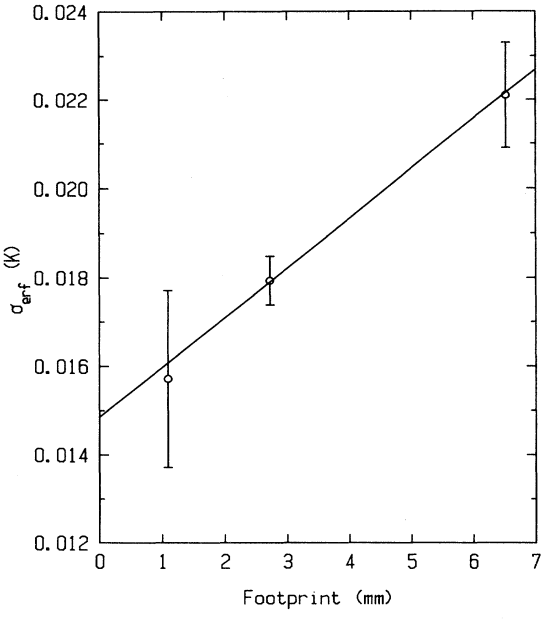

FIG. 7. The widths of error-function fits to temperature scans as a function of the x-ray footprint size on the sample of $x = 0.263$ BA in 12CB. The slope is equivalent to a temperature gradient of 1.118 mK/mm; the fact that the intercept is at positive width σ_{erf} shows that either the transition has an intrinsic width of $\sigma_{erf} = 0.0149$ K or that other inhomogeneities—on small length scales or transverse to the beam—broaden a sharper transition.

The temperature dependence and position dependence of the reflectivity suggests that a true first-order transition could be taking place, but at different temperatures along the surface, due to temperature or composition gradients, as expressed by $R(0.15\ \text{Å}^{-1}, T - T_{eff}(X))$. This would lead to a measured nonzero width of the transition, due to the finite portion of the sample illuminated by x rays. To explore this, temperature scans were performed with x-ray footprints of 6.5 mm, 2.7 mm, and 1.1 mm, and an error function was fitted to the step in $R(0.15\ \text{Å}^{-1}, T)$ corresponding to $j = 1 \rightarrow j = 2$. The fitted error-function widths of these scans are displayed in Fig. 7. The linear fit is reasonable, and has an intercept of $\sigma_{\text{erf}} = 0.015 = \pm 0.003$ K. The slope is $|d\sigma_{\text{erf}}/dX| = 1.1$ mK/mm, very close to the estimate for $|dT_{eff}(X)/dX|$ above.

The residual width of 0.015 K could express the fact that the transition is not first order, or that the same apparent temperature or composition gradients evidenced by the sample scans are also present in the lateral direction, where the intensity is averaged by the 5 mm wide footprint.

What is the source of the apparent gradient in $T_2(X)$? Temperature gradients are unlikely, as it was previously verified through measurements with calibrated thermistors that temperature gradients from the center to the edge of the sample were $|\Delta T| \leq 0.005$ K, whereas the value of dT_2/dX above would lead to a 0.07–0.1 K temperature gradient across the entire sample. On the other hand, a concentration gradient of $dx_0/dX = (1.8\text{–}2.2) \times 10^{-5}$ mm^{-1} would have the same effect as a temperature gradient. At present we do not understand the origin of this behavior for higher concentration samples.

In summary, we have found that the addition of BA to 12CB reduces both the bulk transition temperature T_{IA} and surface transitions temperatures T_j nearly linearly with concentration; BA "sharpens" the layering transitions evidenced in $R(0.15\ \text{Å}^{-1}, T)$; and that we can make good fits to the data using a model where the only significantly changing parameter is A_2, the amplitude of the second layer. In particular, while the thickness d does change as a function of temperature to well outside the fitted error bars, the *relative* change of A_2 across the transition is much larger—an increase of over a factor of 4 as temperature is lowered. To a first approximation the change in the full reflectivity, and in the constant-q_z $R(0.15\ \text{Å}^{-1}, T)$, can be understood to be an effect of A_2 alone. This last observation will be used in the Landau theory analysis of Sec. V.

B. 10CB and 10CB-BA mixtures

For pure 10CB, two samples were measured, with bulk transition temperatures of $T_{IA} = 50.429 \pm 0.005\,^{\circ}$C and $T_{IA} = 49.975 \pm 0.005\,^{\circ}$C. A single concentration of BA in 10CB, $x_0 = 0.274$, was measured in two samples as well, with bulk transition temperatures of $T_{IA} = 32.278 \pm 0.005\,^{\circ}$C and $T_{IA} = 32.349 \pm 0.005\,^{\circ}$C.

Specular reflectivities for pure 10CB were measured at 14 reduced temperatures ranging from $t = 1.19 \times 10^{-3}$ to

$t = 2.144 \times 10^{-2}$; nine reflectivities for the first sample and five for the second. For the mixtures, specular reflectivities were measured for 21 temperatures in the range $t = 1.9 \times 10^{-4}$ to $t = 1.4 \times 10^{-1}$; 17 for the first sample and four for the second sample.

In both cases, these concentrated on the region of the $j = 1 \rightarrow j = 2$ transition, as determined through model fits. The form of the specular reflectivities is quite similar to that for pure 12CB in Fig. 2, but with the primary maximum shifted to larger q_z, due to the smaller layer spacing in 10CB. Also, because the number of layers at the lowest temperatures was significantly greater than in 12CB (10 for pure 10CB, 5–6 for pure 12CB), this maximum showed a greater intensity than in pure 12CB at the lowest temperatures. Data for temperatures significantly below $j = 1 \rightarrow j = 2$ will not be discussed here.

Figure 8 shows the curves $R(q_z^* = 0.1675\ \text{Å}^{-1}, t)$ for 10CB and 10CB-BA. Both curves are significantly different than the measurements $R(0.15\ \text{Å}^{-1}, t)$ in 12CB and 12CB-BA. First, for both the changes in intensity which were found to signal the addition of layers occur at significantly higher reduced temperature than for the longer molecule. Second, the changes in intensity are far less localized than for the 12CB samples: gone are the steplike changes which signal the discrete addition of layers, replaced in the case of pure 10CB by a gradual increase in intensity (for $j > 1$) upon which are superimposed small variations that can be identified with layer growth. There are two immediately apparent similarities with the 12CB and 12CB-BA cases, however: a significant suppression of bulk and surface transition temperatures which leaves the location of features in $R(0.1675\ \text{Å}^{-1}, t)$ virtually unchanged accompanied by a "sharpening" of those features associated with layer growth.

From the appearance of $R(0.1675\ \text{Å}^{-1}, T)$, it would be expected that the temperature dependence of surface smectic order is significantly different than that for 12CB and 12CB-BA. This was verified by fitting the reflectivities using the model electron density Eq. (6); again, the only significantly temperature-dependent parameters are the layer amplitudes A_j.

As with 12CB, the only other model parameter showing significant variation with t is the layer spacing d. There is a large change in d, primarily across the temperature range which the fits associate with $j = 2$ growth ($7 \times 10^{-3} \leq t \leq 2 \times 10^{-2}$). For pure 10CB at the highest temperatures, the thickness is $\bar{d} = 32.18 \pm 0.12$ Å. Below $j = 2$ saturation, d reaches a plateau of $\bar{d} = 34.58 \pm 0.01$ Å. For $t \leq 3 \times 10^{-3}$, where further layers are growing, there is no significant change in d. As with 12CB, this is significantly smaller than the bulk spacing of $d = 35.36$ Å. For 10CB-BA, d also shows some temperature dependence, *increasing* from $d \approx 31$ Å to $d \approx 34.5$ Å as temperature was lowered through $j = 1 \rightarrow j = 2$.

For pure 10CB, the position of the center of the first

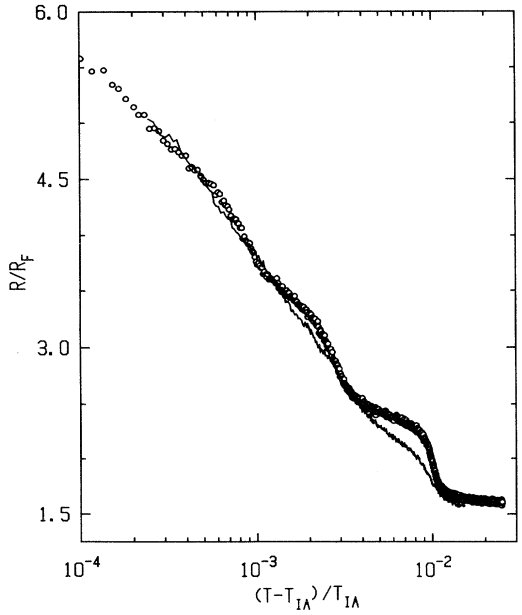

FIG. 8. Normalized reflectivity $R(0.1675\ \text{Å}^{-1}, t)$ for pure 10CB (·) and $x_0 = 0.174$ BA in 10CB (○). The dramatic "sharpening" of the apparent transitions illustrates an effect analagous to that of BA in 12CB.

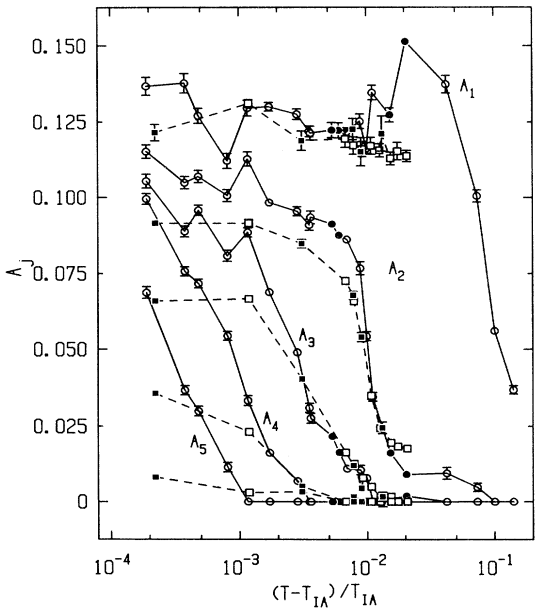

FIG. 9. Layer amplitudes for pure 10CB (□, sample 1, □, sample 2) and $x_0 = 0.247$ BA in 10CB (○, sample 1, •, sample 2) as obtained from fits to the independent-layer model. Amplitude A_1 is nonzero for all temperatures, even as high as 30 K above T_{IA}. Though A_1 shows some variation in the temperature region over which A_2 changes for both pure 10CB and 10CB-BA, it is essentially constant below $t \approx 5 \times 10^{-2}$. Only A_3 shows appreciable variation before A_2 saturates. Amplitudes A_3, A_4, and A_5 show a substantial region of simultaneous growth.

bilayer, z_0, was nearly constant for each sample, though there was a significant sample-to-sample difference. For sample 1, the average is $\overline{z_0} = 18.05 \pm 0.03$ Å, while for sample 2 it is $\overline{z_0} = 17.13 \pm 0.04$ Å. The larger value for sample 1 could be due to the presence of surface contamination, though the difference in z_0 is somewhat smaller than what one would expect for even a small organic contaminant (at least 2–3 Å). If due to contamination, this difference shows that impurities which are surface specific do not significantly affect the layering behavior.

The surface roughness σ_s as a function of t shows a gradual change from $\sigma_s = 4.54 \pm 0.04$ Å to $\sigma_s = 4.82 \pm 0.05$ Å as temperature is reduced.

For 10CB-BA, there is a great deal of variation in z_0 which is not attributable to the different samples; this is true of σ_s as well. The consistency of A_2 and d values suggests that the variations in z_0 and σ_s may be attributable to systematic errors or inadequacies of the model; these deficiencies do not seem to reduce the model's sensitivity to the the layer spacing or amplitudes, which show remarkable consistency between samples.

Figure 9 shows the fitted layer amplitudes A_1–A_5 as a function of reduced temperature for 10CB and 10CB-BA. As expected, the changes in slope of $R(0.1675\ \text{Å}^{-1}, t)$ are accompanied by changes in A_3 and A_4 as well. Layer 1 is seen to be essentially constant below $t = 5 \times 10^{-2}$. Amplitude A_2 is the only amplitude which grows to near saturation without appreciable simultaneous growth of other layers. Even while A_2 is changing significantly, there is some growth of A_3 and A_4. As indicated in the figure, the differences between samples of the same composition are on the order of the fitted error bars.

V. LANDAU THEORY FOR $j = 1 \rightarrow j = 2$

The simplest applications of Landau theory are not expected to be able to produce the incomplete smectic wetting phase diagram of long-chain liquid crystals because there is no clear way for such continuum theories to produce the discrete, well-separated layering transitions experimentally observed [21]. However, the conceptual and computational simplicity of Landau theory, and the lack of compelling agreement between experiment and other existing mean field theories [21–25], argue in favor of its use.

Furthermore, by focusing on the growth of a single layer, the difficulty of describing discrete layer formation is avoided. As shown above, in the vicinity of $j = 1 \rightarrow j = 2$ in 12CB, the topmost layer is saturated, while there is virtually no order in the third layer. For this restricted problem, the remainder of the material may be ignored.

The free energy which must be minimized is taken to be of Landau–de Gennes form [39], with an additional surface term of the form $F_s \sim -h(z)|\psi(\mathbf{r})|$, where $h(z)$ is a surface field and F_s is taken to be negative to promote surface order. Since the problem is to be solved in mean field approximation, and we assume that there is no dependence on coordinates parallel to the interface, we can write $\psi(\mathbf{r}) = \psi(z)$. A further approximation is to discretize the z axis, so that the order parameter becomes $\psi(z) = \psi_1(z_1), \psi_2(z_2), \ldots$, where z_i is the position of the ith layer. This approximation appears to be valid for 12CB and 12CB-BA, where the $\psi_1 \approx$ const and $\psi_3 \approx 0$ in the temperature range of interest. Using this approximation and taking $\psi(z)$ real, the free-energy expansion for the second layer becomes

$$F(P,T,\psi_2) - F(P,T,0) = \frac{1}{2}A_0(T - T_c)\psi_2^2 + \frac{B}{4}\psi_2^4 + \frac{C}{6}\psi_2^6 - h\psi_2. \quad (7)$$

The lowest order temperature dependence has been included in the coefficient of the ψ_2^2 term, $A(T) \equiv A_0(T - T_C)$.

In the case of a mixture, the free energy must be expressed in terms of two order parameters, ψ_2 and the concentration (mole fraction) of the solute, $x = n_{sol}/(n_{sol} + n_{lx})$, where the n's are number densities of the solute and liquid crystal. If the region of interest is far from a phase transition in the pure solute, solute-solute interactions can be ignored [20]; this leaves us with a coupling between order parameters. The simplest allowed coupling is $F_C \sim x\psi_2^2$, which is positive (this yields a suppression of the transition temperature for $x > 0$).

Additional terms arise depending on the thermodynamic ensemble used for the calculation. For a bulk transition in a puddle at constant P and adjustable temperature T, P and T are independent variables. Assuming negligible vapor pressure for both solute and solvent, the total concentration x is constant. The correct energy is then the Gibbs free energy, $G(P,T,\psi_2,x)$, with an entropy of mixing term.

Because a solution using the Gibbs free energy is difficult, an approximation valid for surfaces can be employed. As in the freezing of a liquid containing impurities, a region of two-phase coexistence is expected, one phase being solute rich or "unfrozen" (I), the other solute poor or "frozen" (smectic A). For smectic order at the surface of a macroscopic puddle, the smectic region contains on the order of 1 part in 10^5 of the total number of molecules. Approximating the bulk as an infinite reservoir of solute and solvent, the appropriate ensemble is the grand canonical ensemble, in which chemical potential, not particle number, is fixed.

The correct free energy is the grand potential, Ω:

$$\begin{aligned}\Delta\Omega(P,T,\psi,\mu) &= \Omega(P,T,\psi,\mu) - \Omega(P,T,0,\mu) \\ &= \frac{1}{2}A(T)\psi^2 + \frac{1}{4}B\psi^4 + \frac{1}{6}C\psi^6 - h\psi \\ &\quad + \frac{1}{2}Dx\psi^2 + RTx(\ln x - 1) - \mu_0 x, \quad (8)\end{aligned}$$

where μ_0 is the chemical potential of the solute given an infinite reservoir of particles. Above and for the remainder of the discussion, $\psi_2 \rightarrow \psi$.

At high temperatures in the I phase ($\psi = 0$), minimization with respect to x yields μ_0, which may be substituted into Eq. (8) when $\psi \neq 0$, since the chemical potential is fixed. Minimizing Eq. (8) with respect to x for $\psi \neq 0$ yields

$$x = x_0 e^{-D\psi^2/2RT}. \quad (9)$$

Substitution into Eq. (8) gives

$$\Delta\Omega = \frac{1}{2}A(T)\psi^2+\frac{1}{4}B\psi^4+\frac{1}{6}C\psi^6-h\psi-RTx_0e^{-D\psi^2/2RT}, \tag{10}$$

and the equilibrium value of ψ is given by the solution to

$$\frac{\partial\Delta\Omega}{\partial\psi} = A(T)\psi+B\psi^3+C\psi^5-h+Dx_0\psi e^{-D\psi^2/2RT} = 0. \tag{11}$$

Equation (11) does not give ψ in closed form; the solution must be found numerically. However, if $D\psi^2/2RT$ is small in the region of interest, the exponential can be expanded, giving

$$\Delta\Omega = \frac{1}{2}A'(T)\psi^2+\frac{1}{4}B'\psi^4+\frac{1}{6}C'\psi^6-h\psi-RTx_0. \tag{12}$$

The new coefficients are

$$\begin{aligned} A'(T) &= A_0(T-T_C'), \\ T_C' &= T_C-\frac{Dx_0}{A_0}, \\ B' &= B-\frac{D^2x_0}{2RT}, \\ C' &= C+\frac{D^3x_0}{8R^2T^2}. \end{aligned} \tag{13}$$

Having restored the free energy to Landau form, the usual statements regarding the role of the coefficients may now be made [40]. For $h = 0$ and $B' > 0$, the transition is second order and occurs at $t = T - T_C' = 0$; in the immediate vicinity of the transition,

$$\psi = \begin{cases} 0, & t > 0 \\ |\frac{A_0 t}{B'}|^{1/2}, & t < 0. \end{cases} \tag{14}$$

The addition of $h > 0$ results in a continuous transition without a simple power-law dependence of ψ on t.

If $B' = 0$, the transition for $h = 0$ is at the tricritical point, and $\psi \sim |t|^{1/4}, t < 0$. Finally, for $B' < 0$, the transition becomes first order, with a jump from $\psi = 0$ to $\psi \neq 0$ at a transition temperature

$$T^* = T_C+\frac{3B'^2}{16A_0'C'}. \tag{15}$$

Again, for $h > 0$ the transition is still first order, but a numerical solution shows pretransitional growth of ψ due to the influence of the external field.

There are three immediate consequences of Eqs. (9), (13), and (15). First, the transition temperature is suppressed linearly with solute concentration for a second-order transition, and nearly linearly but with a small correction for a first-order transition; this agrees qualitatively with the experimental dependence of both T_{IA} and T_2 on x_0. Second, if B is positive at zero concentration, B' can be driven negative as solute is added, causing a second-order transition to become first order; in any case, the addition of impurities causes the transition to have a more first-order character. Finally, the growth of smectic order is accompanied by separation into a solute-rich (I) region and a solute-poor (smectic-A) region: solute is "expelled" from the region in which smectic order grows.

The results of the independent-layer fits were used for an analysis using the full Landau theory expression Eq. (11). For this analysis, the second-layer amplitude A_2 ($\equiv \psi$) must be determined over a significant temperature range and with sufficient point density to clearly show relatively small changes in shape with changing concentration of solute. To measure and analyze many reflectivities is not only tedious, but introduces uncertainties due to temperature drifts and systematic errors. An alternative is to extract A_2 directly from the temperature scans. We found that a simple scaling method based on measuring $R(0.15\ \text{Å}^{-1}, t)$ and two reflectivities, one at a temperature above $j = 1 \rightarrow j = 2$ and one below the transition, produced results which agreed with the independent-layer analysis to within the error bars of the fitted A_2 values.

First, two full reflectivities at reduced temperatures t_a, t_b were obtained and fitted to the reflectivity modeled by the electron density of Eq. (6). The temperature scan $R(0.15\ \text{Å}^{-1}, t)$ was then fitted to a form composed of an error function and a polynomial to provide values of R at t_a and t_b; any smooth fit would suffice, as long as interpolation between the experimental points in t can be done. The curve R was then scaled by multiplication and addition of a constant offset to yield $R_{\text{scale}}(t_a) = A_2(t_a)$ and $R_{\text{scale}}(t_b) = A_2(t_b)$. Figure 10 shows the result for pure 12CB; similar results were obtained for $x_0 = 0.145$.

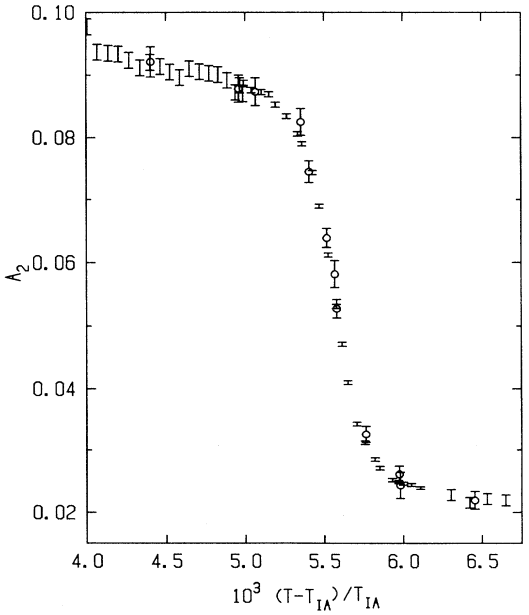

FIG. 10. Comparison between A_2 for pure 12CB as fitted in the independent-layer model (○) and simple scaling method for obtaining A_2 from $R(0.15\ \text{Å}^{-1}, t)$ (·).

As can be seen, this method yields excellent agreement with A_2 as determined from the reflectivity fits. Assuming that this method provides a one-to-one mapping from $R \rightarrow A_2$, the error bars have been scaled from R in the same way as R. The procedure was applied to all concentrations, and the resultant A_2 data used in the analysis.

Two modifications were made to the Landau theory prior to fitting. First, it was found that good fits could be obtained for temperatures below the center of the transition only if an eighth-order term $E\psi^8/8$ were included in the free-energy expansion. In view of the fact that the best indication of the order of the transition is the shape in the pretransitional region on the high-temperature side, it is fortunate that the effect of the eighth-order term in this region is negligible. In addition, since the temperature dependences of all of the order parameters, for all samples with $x_0 \geq 0.118$, appear to be essentially a step function with a common temperature smear, the data were fitted to the convolution of the Landau theory with a Gaussian of temperature width σ_T.

If the Landau theory is to be used to describe the effects of solutes on the $j = 1 \rightarrow j = 2$ layering transition, the coefficients, the coupling to concentration, the external field, and T_C in Eq. (11) should be common to all samples. This presents some difficulty given the experimental results, in that the suppression of T_2 with increasing concentration is not smooth, but shows a good deal of scatter (see Fig. 4). Because of this scatter, the concentration x was allowed to vary slightly from x_0. This appears to be justified by the rather large variation in T_{IA} observed for a number of samples mixed to have the same nominal x_0 which presumably reflects uncertainties in initial concentration. Furthermore, slight changes in concentration primarily affect the transition temperature T^* and not the *shape* of the transition.

In these fits, all A_2 sets were fit simultaneously with the following common parameters: coefficients A_0, B, C, and E; the external field strength h/A_0; the second-order coefficient coupling A_2^2 to x, D/A_0; the temperature at which the second-order coefficient in pure 12CB changes sign, T_C; and the temperature smear σ_T. In addition, for pure 12CB there were two sample-dependent parameters, a constant background $\mathcal{B}$ and a linear temperature dependence $\mathcal{L}$; the latter was included only to fit the values of A_2 at the highest temperatures, and has virtually no effect on the shape of the fitted curve in a region of ± 0.5 K around the center of the transition. For samples with BA, the sample-dependent parameters were the concentration x, a constant background $\mathcal{B}$, and a scale factor S. The effect of the scale factor is to produce a fitted curve, $A_2^{\text{fit}} = SA_2^{\text{Landau}}$; if the Landau theory describes the data well, a correct choice of common parameters would yield $S = 1$ for all samples.

The linear suppression of T_2 with x_0 shows that the likewise linear renormalization of T_C' in Eq. (13) dominates the change in transition temperature. Based on this observation, the fitted slope of T_2 vs x_0 supplies an initial guess value of $D/A_0 = -64$ K/mole fraction.

The data used for the Landau theory analysis are shown in Fig. 11, along with the Landau theory fits. The curves have been offset for greater clarity, and both fits and data have been rescaled by $1/S$ to give uniform scaling. The solid lines are the fits with temperature smear, while the broken lines show the curves without temperature smear.

The common parameters of the fits are given in Table II and the sample-dependent parameters in Table III. The relative errors in both the common parameters and the sample-dependent parameters are of the order of 1% or less; this, however, is based on the error bars produced from the temperature scans by scaling, which do not include the errors introduced by the scaling. But if we assume that the temperature scans reflect primarily the temperature dependence of A_2, the errors used for these fits should not be gross underestimates.

The important sample-dependent parameters are the fitted concentration x and the scale S. Again, the concentration was fitted to give the correct transition temperature within the model. It was found that the fitted concentration for samples with $x_0 \geq 0.145$ was within 5% of the nominal value, while that for lower concentrations differed from the nominal values by 15–20 %. This could be a result of the drifts, which were of the same magnitude for all samples: relative uncertainties in concentration due to drifts would be larger for small concentrations than for large concentrations. The only noticeable effect of small discrepancies between fitted x and nominal x_0 is

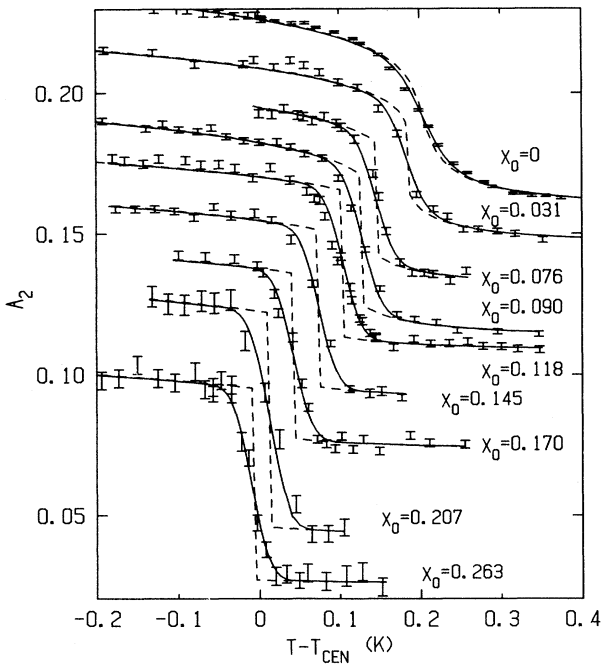

FIG. 11. Landau theory fits to the order parameter A_2 at the $j = 1 \rightarrow j = 2$ transition, with BA concentrations as shown. The solid lines represent the fits including a temperature smear of $\sigma_T = 0.018$ K; the broken lines show the fitted order parameter in the absence of smearing. The fitted temperature of the center of the transition, T_{CEN}, has been subtracted, and the curves have been offset horizontally and vertically for clarity.

TABLE II. Landau theory fit—common parameters. Common parameters for the Landau free-energy density used to fit the temperature dependence of A_2 (ψ). The parameters are the coefficients $A_0(\psi^2)$, $B(\psi^4)$, $C(\psi^6)$, $E(\psi^8)$; the coupling to concentration of BA, D/A_0; the surface field h/A_0; and T_C, defined by the second-order coefficient $A = A_0(T - T_C)$.

A_0	$6.98 \times 10^5 \pm 3 \times 10^3$
B	$4.04 \times 10^6 \pm 1.6 \times 10^4$
C	$-5.17 \times 10^9 \pm 2 \times 10^7$
E	$2.426 \times 10^{12} \pm 6 \times 10^9$
D/A_0	64.26 ± 0.6
h/A_0	$-8.67 \times 10^{-4} \pm 3.4 \times 10^{-6}$
T_C	333.080 ± 0.002

a shift in the transition; shape changes sufficient to degrade the quality of the fits for this data are not created by these changes in x.

The average scale factor S was slightly smaller than 1.0, $\overline{S} = 0.95$. This means that the experimentally determined magnitude of the change in order parameter across the transition is smaller than the model prediction. In principle, it is possible to change this by making the coefficient E more positive, so that saturation occurs at a slightly smaller value of the order parameter. In practice, this procedure yielded poor fits. Also, the deviation of S from 1.0 is not systematic; if the model overestimated the change in A_2, S would monotonically decrease with increasing concentration. The spread in values of S could be the result of systematic errors in the scaling procedure used to generate the data from the temperature scans or sample-to-sample differences not entirely attributable to the presence of BA (such as impurities on the surface). Regardless of these systematic errors, the fact that $\overline{S} \approx 1.0$ is indicative that the choice of common parameters for the fits is good.

The important results can be easily seen in Fig. 11. As with $R(0.15\ \text{Å}^{-1}, T)$, the greatest changes in shape occur for fitted $x \leq 0.118$.

We note first that the temperature smear σ_T has almost no effect on the pure 12CB fit. Furthermore, A_2 for 12CB with no temperature smear is continuous, showing that the transition is second order. All other concentrations without σ_T show a significant jump ΔA_2 which accounts for more than half of the total change in A_2 around the transition for concentrations as low as $x_0 = 0.076$. This results from the fact that the second-order coefficient B' is driven strongly negative for even the $x_0 = 0.031$ sample. This means that the transition is continuous ("second order") for pure 12CB, while it is discrete ("first order") for all nonzero concentrations measured. Also apparent is the fact that the *shapes* of data and fits for $x_0 \geq 0.118$ are virtually identical: pre- and post-transitional effects have been suppressed, and the primary effect of increasing concentration is the suppression of the temperature of the transition.

Saturation for larger concentrations is also apparent in the jump in order parameter ΔA_2, as shown in Fig. 12. The fit parameters which yield a continuous transition for pure 12CB predict that the crossover to first-order behavior occurs at a very small concentration, $x \approx 0.016$. This would be analogous to a tricritical point in the bulk. Another possibility, to be discussed below, is that pure 12CB is near the critical point for $j = 1 \rightarrow j = 2$, and

TABLE III. Landau theory fit—individual parameters. Sample-dependent parameters used to fit the temperature dependence of $A_2(\psi)$ with the Landau free-energy density. For each nominal concentration x_0 of BA, the fitted parameters are the concentration x; the constant background $\mathcal{B}$; and the scale factor S. Also given are the χ^2 values for the individual fits.

x_0	x	$\mathcal{B}$	S	χ^2
0	0	0.67 ± 0.05	1	3.499
0.0314	0.03576 ± 0.00007	0.2043 ± 0.0006	0.92 ± 0.01	2.849
0.0761	0.065421 ± 0.000001	0.0220 ± 0.0007	0.93 ± 0.01	1.554
0.0904	0.07179 ± 0.00008	0.0303 ± 0.0006	1.02 ± 0.01	2.27
0.1181	0.132021 ± 0.000004	0.0175 ± 0.0007	0.96 ± 0.01	3.784
0.1446	0.1469 ± 0.0002	0.0199 ± 0.0009	0.88 ± 0.01	1.705
0.1702	0.177985 ± 0.000003	0.0176 ± 0.0009	0.89 ± 0.02	4.855
0.2067	0.21020 ± 0.00007	0.014 ± 0.005	1.06 ± 0.02	1.888
0.2631	0.26190 ± 0.00006	0.024 ± 0.001	0.91 ± 0.02	0.938

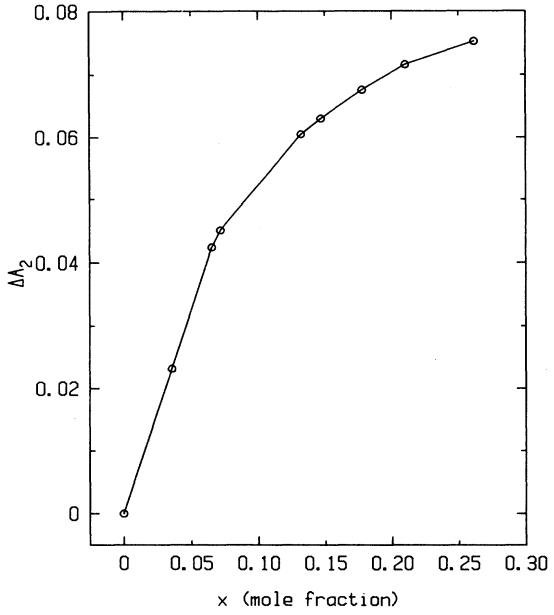

FIG. 12. Jump in order parameter ΔA_2 at the transition as a function of fitted concentration x from the best-fit Landau theory parameters. Only pure 12CB shows no discontinuity in A_2.

that the addition of impurities causes the phase diagram to shift in such a way that this critical point is crossed by scanning T at constant P for $x = 0.016$.

The fact that $j = 1 \rightarrow j = 2$ appears to be continuous only in pure 12CB is cause for some suspicion that the fits have fortuitously provided a crossover such that all nonzero concentrations of BA measured are first order. Attempts were made to vary the parameters of the model to determine whether other satisfactory fits could be obtained; the details are not important, but we found that we could neither remove the temperature smear nor change the coefficients in such a way as to make all, or at least more, transitions continuous.

In summary, the best fit to the Landau theory model is one in which (a) there is a temperature smear of 0.018 K; this is consistent with the discussion above regarding the inhomogeneous surface structure for high-concentration samples and the asymptotic value of the width of an error-function fit to $R(0.15\ \text{Å}^{-1}, T)$; (b) the transition is continuous for pure 12CB, but discontinuous for all other samples; and (c) the effect of added impurities on the shape of the transition is negligible for $x_0 \geq 0.118$.

VI. DISCUSSION

What is most striking about the surface smectic structure of pure 12CB and 12CB-BA is not their differences, but their similarities. This can be easily seen by looking at both the reflectivities and fitted electron-density profiles for pure 12CB and $x_0 = 0.145$ BA in 12CB at temperatures above and below the $j = 1 \rightarrow j = 2$ transition, as shown in Fig. 13. There is only one systematic difference in the fitted parameters of the independent-layer model, other than the temperature dependence of A_2. This is that the layer spacing d for the mixtures is ≈ 0.7 Å smaller than that of pure 12CB in the $j = 2$ region. Other than this, the electron density is for the most part insensitive to the presence of BA.

Where *would* one expect the BA molecules to reside in the layers? Firstly, both 12CB and BA have significant dipole moments, $\mu_D = 4.95$ D for 12CB [41] and $\mu_D = 5.54$ D for BA [42]. Furthermore, experiments on the homologous series nCB indicate that the dipole moment is primarily associated with the cyano-terminated aromatic core [41]. As a result, preferential association of BA with the core region might be expected.

Experiments addressing solute location in smectic liquid crystals are inconclusive. Moseley and Lowenstein [36] used ^{13}C NMR to study the anisotropic diffusion of methane and chloroform in a number of liquid crystals, including 7CB and 8CB. They found that the diffusion constant for motion parallel to the layers in the A phase was 2–5 times greater than that for perpendicular motion. By using packing and chemical affinity arguments,

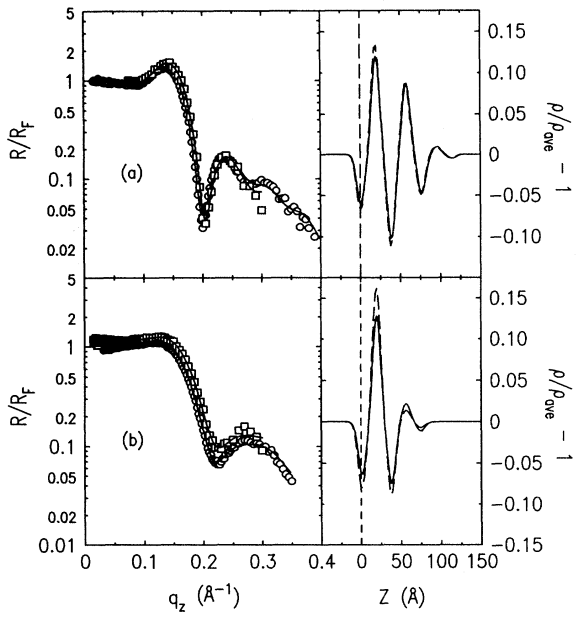

FIG. 13. Reflectivities R/R_F, and the fitted electron densities of pure 12CB (○) and $x_0 = 0.145$ BA (□) in the $j = 2$ region (a) and $j = 1$ region (b). The error function used to model the liquid-vapor interface has been removed from the electron densities for clarity. The reduced temperatures of the pure 12CB are $t = 5.07 \times 10^{-3}$ (a) and $t = 6.46 \times 10^{-3}$ (b), while those for the mixture are $t = 4.55 \times 10^{-3}$ (a) and $t = 8.43 \times 10^{-3}$ (b). Aside from the amplitude A_1 at higher temperatures, the profiles for pure 12CB (——) and the mixture (– –) in each region ($j = 1$ or $j = 2$) are virtually identical.

this was attributed to the expulsion of solute from the core region into the aliphatic tails, in the case of nonpolar methane, or an enhanced affinity for the core in the case of polar chloroform. In either case, motion perpendicular to the layers is impeded, while motion parallel to the layers allows the solute to remain in a region of high solubility.

On the other hand, the experiments of Guo and Fung [43] seem to indicate no preferential association. These ^{13}C NMR experiments used variable-angle spinning (VAS) and separated local field (SLF) spectroscopy to determine the nematic order parameter of different parts of the 7CB and 8CB molecules. No appreciable change in *orientational* order in either the cores or tails due to the addition of $x = 0.08$ CCl_4, cyclohexane, benzene, or hexane was observed. Because an affinity for one part of the liquid crystal molecule might be expected to enhance or disrupt the order of that region, they interpret their findings as evidence that preferential association does not occur.

Finally, it is possible that BA is at least partially expelled from the surface smectic layers, in analogy to bulk phase separation of a mixture. The above-cited NMR studies showed no indication of bulk phase separation in mixtures, as indicated by a lack of hysteresis; this is in contrast to the our experience with the *bulk* 12CB-BA transition. The difficulty we observed in remixing the samples after bulk phase separation, which is reasonable given typical diffusion constants in smectics, should not be a problem as far as phase separation in the surface region is concerned: the expulsion of BA as temperature is lowered, and subsequent reincorporation upon heating, could proceed rapidly because of the thinness of a surface region in contact with a bulk BA reservoir.

Experimentally, we were not able to determine any signs of phase separation in the surface region. Because the bulk electron densities for for 12CB and BA differ by only a few percent, we expect that the any differences in average electron densities between BA-depleted and BA-rich regions would be quite small. Though reflectivity is sensitive to small variations in electron density, we feel that the imperfect nature of the model used to fit the reflectivity, as well as the large number of adjustable parameters, make it unlikely that we could demonstrate such an expulsion effect for the current materials.

The most significant effect of the solute is to alter the temperature dependence of the $j = 1 \rightarrow j = 2$ layering transition, as well as lowering the bulk T_{IA} and the individual T_j. The same qualitative effects were seen in 12CB-BA and 10CB-BA mixtures: a "sharpening" of the features in $R(q_z^*, T)$ which we have called layering "transitions" and an overall suppression of the temperatures such that t_j are roughly the same for pure materials and mixtures.

The inhomogeneous reflectivities for $x_0 > 0.145$ BA in 12CB are a cause for concern, because they complicate the interpretation of the temperature dependence of the smectic amplitude A_2. However, it should be stressed that the effects are consistent from sample to sample. As discussed above, the largest possible temperature gradient across the entire sample was of the order of $|\Delta T| \leq 5$ mK. This alone would be insufficient to cause a broadening of a first-order transition by a few tenths of a degree across the surface of the sample. If the temperature gradient drives a concentration gradient, this would magnify the effect. If, on the other hand, the inhomogeneous reflectivities are the result of an incomplete initial mixing of 12CB and BA, the expected diffusion of BA in 12CB would not be significant on the time scales of the experiments at the temperatures studied. In such a case, no progressive lessening of the inhomogeneities would be observable.

Sample curvature effects could also be implicated in this regard. A simple analysis [44] shows that the relative change in surface tension due to the expected curvature at the edges of the sample should be of the order of $\Delta|\gamma/\gamma_0 - 1| \approx (2\text{–}5) \times 10^{-6}$, where γ_0 is the surface tension at the center of the transition. A recent surface tension measurement [45] of pure 12CB shows that the relative change in surface tension over a region of about 0.25 °C at the transition—the extent of the inhomogeneities—is $\Delta|\gamma/\gamma_0 - 1| \approx 2.5 \times 10^{-3}$. Clearly, curvature alone is not likely to be responsible for the inhomogeneities. However, it is possible that sample curvature drives a concentration gradient, in which BA is depleted from the regions near the edges of the sample.

Though the source of these inhomogeneities is unknown, inspection of the scans $R(0.15\ \text{Å}^{-1}, t)$ shows that the layering grows increasingly sharp up to $x_0 = 0.118$ BA. Even in the presence of the inhomogeneities, if a temperature broadening of 0.018 K is assumed, consistent with the observed position dependence of the transition on the sample surface, the transition appears to become completely first order with a concentration of $x_0 = 0.118$; there is very little change in $R(0.15\ \text{Å}^{-1}, t)$ for higher concentrations.

The behavior of the second-layer amplitude A_2 is consistent with a Landau theory which was used to simultaneously fit data for nine concentrations of BA in 12CB. The observations borne out by this model include a nearly linear suppression of the transition temperature T_2; a sharpening of the transition, due to the reduction of smectic susceptibility with increasing concentration; and a larger change ΔA_2 of the order parameter across the transition. The parameters of the Landau theory indicate that the transition in pure 12CB is continuous, but that the effects of the surface field and/or presence of $A_1 \neq 0$ cause a pretransitional tail; and that the addition of as little as 1% BA drives the transition first order.

While the theory has not been applied to 10CB, it is qualitatively clear that a concentration of $x_0 = 0.274(10\%)$ BA in 10CB still leaves a significant breadth to the transition, of the order of ≈ 1 °C. This width is significantly larger than the range of the inhomogeneities in reflectivity for 12CB-BA (≈ 0.25 °C), and is unlikely to be an artifact; furthermore, the reflectivity inhomogeneities were not observed for 10CB-BA. As a result, $x_0 = 0.274(10\%)$ BA has probably not driven the $j = 1 \rightarrow j = 2$ transition first order. To correctly apply the theory to 10CB would require the use of at least two order parameters, A_2 and A_3, because of the significant

growth of A_3 in the temperature range over which A_2 grows to saturation.

The theory also predicts what one would intuitively expect, that solute should be expelled from a region as smectic order develops there. In the theory,

$$x(\psi) = x_0 e^{-D\psi^2/2RT}. \quad (16)$$

This implies that $\approx 8\%$ of the BA in the $j = 2$ region of the surface is expelled when the sample goes through the $j = 1 \rightarrow j = 2$ transition for the highest-concentration 12CB-BA sample. As discussed above, however, the lack of scattering contrast between 12CB and BA would make the detection of such a small effect difficult.

Among other issues, future work should address this possible phase separation. The use of a solute with a greater electron density may be sufficient for this. Simulations show that the *complete* expulsion of a perfluorinated BA, pentafluorobenzyl alcohol (PFBA), from the surface of a mixture with bulk concentration of $x_0 = 0.24$ would cause features in the x-ray reflectivity characteristic of the length scale over which the depletion occurs. Preliminary measurements on one sample of $x = 0.24$ PFBA in 12CB were inconclusive: the data could not be fitted well with the independent-layer model as described above, but no limits on concentration differences between the surface smectic region and the isotropic bulk could be determined. This is not surprising if the expulsion reduces the concentration of solute by less than 10%. Unfortunately, samples with higher concentrations of PFBA showed the same instabilities as high concentrations of BA, precluding studies that might have enhanced the hypothesized electron-density difference.

Another way of addressing this issue would be to use a solute with an atom which has an absorption edge whose wavelength is accessible at a synchrotron x-ray facility. By measuring the anomalous reflectivity with x-ray wavelengths just below and just above the absorption edge, it should be possible to reconstruct the depth profile of the atomic species of interest. A further promising possibility would be selective deuteration of solute or liquid crystal molecule for neutron reflectivity measurements. The large scattering-length contrast created in this way should allow the determination of solute concentration in the surface layers.

A further aspect of possible expulsion of material from the surface for 12CB has interesting implications for high-concentration mixtures, because these samples show smectic order at the surface at temperatures well below the material's *bulk* crystallization temperature, $T_{AK} \approx 48\,^{\circ}\mathrm{C}$. Grazing-incidence diffraction could be used to examine whether long-range order *within* the plane of the surface exists in the mixtures.

In some respects, the cyanobiphenyl surface-layering phase diagram resembles a generic multilayer-adsorption phase diagram [46]. As shown in previous work [3, 7], short-chain homologs appear to wet continuously and completely, while longer-chain molecules were originally thought to undergo a finite number of first-order layering transitions. In this analogy, short-chain molecules behave like an adsorbing gas which approaches coexistence at high temperatures, above the wetting temperature T_W, while long-chain molecules behave like the gas approaching coexistence below T_W, where it forms a restricted number of solid layers. If this analogy is correct, the individual first-order layering transitions, which exist in the region of incomplete wetting, should be terminated by critical points in a phase diagram expressed in chemical potential and temperature, (μ, T); the presence of critical points has also been suggested by a recent density-functional calculation [25]. When impurities are added, we expect the phase diagram to shift such that the bulk transition occurs at a lower temperature. With this shift, transitions in which layers form continuously can change to true first-order transitions in which new layers form discretely. The result is that the experimental path in which (μ) is held fixed and T varies moves from a position that does not cross a layering phase boundary (i.e., beyond a critical point) to one that cuts across a first-order layer transition line. This is suggested by the behavior of both 12CB and 10CB, but especially 12CB, where a continuous $j = 1 \rightarrow j = 2$ transition appears to become first order with the addition of solute. This implies that the addition of impurities has the same qualitative effect as increasing the chain length. We stress that the evidence for this analogy is merely suggestive at this point, and an exploration of this possibility should be one goal of a more comprehensive study.

A number of other observations from these experiments and our Landau theory analysis suggest directions for further study. Because the $j = 1 \rightarrow j = 2$ transition in 12CB appears to be marginally second order, a quantitative investigation of $j = 0 \rightarrow j = 1$ and $j = 2 \rightarrow j = 3$ should be undertaken, to determine the magnitude of sharpening for those transitions. In addition, the differences between 10CB-BA and 12CB-BA show that chain length could be a useful variable for moving along the μ axis of the surface phase diagram; in particular, measurements of 11CB are of high priority, since the $j = 1 \rightarrow j = 2$ transition for 10CB appears to be continuous even with large concentrations of BA, while that for pure 12CB may be marginally second order and easily driven first order with small amounts of solute. While the surface inhomogeneity problem in 12CB-BA is troublesome, it should be remembered that these effects became apparent only with concentrations significantly in excess of that needed to drive the transition first order. A possible way to test the hypothesis that impurities might push the system away from complete wetting would be to use even shorter-chain homologs, which have been shown to have a larger number of surface layers at the bulk transition. Unfortunately, it was found that bulk phase separation occurs in 9CB-BA when 9CB is in the N phase, so studies would necessarily be confined to $n > 9.3$, where no N phase exists. Still, these effects might be much more pronounced for these shorter molecules. Another study of merit would be of the long-chained nOCB's, which in previous measurements showed layering consistent with incomplete wetting by layers added via first-order transitions [7]. Finally, as discussed above, x-ray reflectivity studies with solutes that possess heavy atoms (with large atomic number Z), or neutron reflectivity studies with deuterated solutes, could provide insight into the distri-

bution of solute molecules within the surface layers, as well as any changes in that distribution as a function of temperature.

ACKNOWLEDGMENTS

The research described here was supported by Grants No. NSF-DMR-91-13782 and No. NSF-DMR-89-20490. Some of the experiments were carried out on the Harvard-BNL liquid surface reflectometer on beamline X22B at the National Synchrotron Light Source, Brookhaven National Laboratory. This facility is supported by DE-AC02-76CH00016. M.D. gratefully acknowledges support by the U.S.-Israel Binational Science Foundation, Jerusalem.

[1] J. Als-Nielsen, F. Christensen, and P.S. Pershan, Phys. Rev. Lett. **48**, 1107 (1982).
[2] P.S. Pershan and J. Als-Nielsen, Phys. Rev. Lett. **52**, 759 (1984).
[3] B.M. Ocko, A. Braslau, P.S. Pershan, J. Als-Nielsen, and M. Deutsch, Phys. Rev. Lett. **57**, 94 (1986).
[4] E.F. Gramsbergen, W.H. de Jeu, and J. Als-Nielsen, J. Phys. (Paris) **47**, 711 (1986).
[5] P.S. Pershan, A. Braslau, A.H. Weiss, and J. Als-Nielsen, Phys. Rev. A **35**, 4800 (1987).
[6] E.F. Gramsbergen and W.H. de Jeu, J. Phys. (Paris) **49**, 363 (1988).
[7] Alan Braslau, Ph.D. thesis, Harvard University, 1988 (unpublished).
[8] B. Ocko, Phys. Rev. Lett. **64**, 2160 (1990).
[9] P.S. Pershan, Phys. Rev E **50**, 2369 (1994).
[10] P.E. Cladis, Wim van Saarloos, David A. Huse, J.S. Patel, J.W. Goodby, and P.L. Finn, Phys. Rev. Lett. **62**, 1764 (1989).
[11] J. Thoen, H. Marynissen, and W. Van Dael, Phys. Rev. A **26**, 2886 (1982).
[12] See W.G. Bouwman and W.H. de Jeu, Phys. Rev. Lett. **68**, 800 (1992), and references therein.
[13] See G. Nounesis, M.J. Young, K.I. Blum, C.W. Garland, and R.J. Birgeneau, Z. Phys. B. **90**, 357 (1993), and references therein.
[14] BDH Limited, Advanced Materials Division.
[15] J. Thoen, H. Marynissen, and W. Van Dael, Phys. Rev. Lett. **52**, 204 (1984).
[16] H. Marynissen, J. Thoen, and W. Van Dael, Mol. Cryst. Liq. Cryst **97**, 149 (1983).
[17] B.M. Ocko, R.J. Birgeneau, J.D. Litster, and M.E. Neubert, Phys. Rev. Lett. **52**, 208 (1984).
[18] B.M. Ocko, R.J. Birgeneau, and J.D. Litster, Z. Phys. B **62**, 487 (1986).
[19] M. Schick, in *1988 Les Houches Lectures, Session XLVIII, Liquids at Interfaces*, edited by J. Charvolin, J. F. Joanny, and J. Zinn-Justin (Elsevier Science Publishers B.V., Amsterdam, 1990), p. 415.
[20] L.D. Landau and E.M. Lifshitz, *Statistical Physics, Part 1*, 3rd ed. (Pergamon, New York, 1980).
[21] Jonathon V. Selinger and David R. Nelson, Phys. Rev. A **37**, 1736 (1988).
[22] Z. Pawlowska, G.F. Kventsel, and T.J. Sluckin, Phys. Rev. A **36**, 992 (1987).
[23] W.L. McMillan, Phys. Rev. A **4**, 1238 (1971).
[24] L. Mederos and D.E. Sullivan, Phys. Rev A **46**, 7700 (1992).
[25] A.M. Somoza, L. Mederos, and D.E. Sullivan, Phys. Rev. Lett. **72**, 3674 (1994).
[26] Michael E. Fisher, J. Chem. Soc. Faraday Trans. 2 **82**, 1569 (1986).
[27] M. Moldover and J.W. Cahn, Science **207**, 1073 (1980).
[28] M. Kahlweigt, G. Busse, D. Haase, and J. Jen, Phys. Rev. A **38**, 1395 (1988).
[29] L.G. Parratt, Phys. Rev. **95**, 359 (1954).
[30] A. Braslau, P.S. Pershan, G. Swislow, B.M. Ocko, and J. Als-Nielsen, Phys. Rev. A **38**, 2457 (1988).
[31] D.K. Schwartz, M.L. Schlossman, E.H. Kawamoto, G.J. Kellogg, and P.S. Pershan, Phys. Rev. A **41**, 5687 (1990).
[32] D. Beysens and M. Robert, J. Chem. Phys. **87**, 3056 (1987).
[33] M.P. Gelfand and M.E. Fisher, Physica (Amsterdam) A **166**, 1 (1990).
[34] B.M. Ocko, X.Z. Wu, E.B. Sirota, S.K. Sinha, and M. Deutsch, Phys. Rev. Lett. **72**, 242 (1994).
[35] A.J. Leadbetter, J.C. Frost, J.P. Gaughan, G.W. Gray, and A. Moseley, J. Phys. (Paris) **40**, 375 (1979).
[36] Michael E. Moseley and Aharon Lowenstein, Mol. Cryst. Liq. Cryst. **90**, 117 (1982).
[37] A.H. Weiss, M. Deutsch, A. Braslau, B.M. Ocko, and P.S. Pershan, Rev. Sci. Instrum. **57**, 2554 (1986).
[38] B. Mahan, *University Chemistry* (Benjamin Cummings, Menlo Park, 1987).
[39] P.G. de Gennes, Solid State Commun. **10**, 753 (1972).
[40] Kerson Huang, *Statistical Mechanics*, 2nd ed. (John Wiley & Sons, New York, 1987).
[41] K.P. Gueue, E. Megnassan, and A. Proutiere, Mol. Cryst. Liq. Cryst. **132**, 303 (1986).
[42] C. Reichardt, *Solvent Effects in Organic Chemistry* (Verlag-Chemie, New York, 1979).
[43] Wen Guo and B.M. Fung, Liq. Cryst. **9**, 117 (1991).
[44] Arthur W. Adamson, *Physical Chemistry of Surfaces*, 5th ed. (John Wiley & Sons, New York, 1990).
[45] X.Z. Wu (private communication).
[46] R. Pandit, M. Schick, and M. Wortis, Phys. Rev. B **26**, 5112 (1982).